Chemical Geology 476 (2018) 280–291

Contents lists available at ScienceDirect

Chemical Geology

journal homepage: www.elsevier.com/locate/chemgeo

The trace element and Sr-Nd-Pb isotope geochemistry of Juan Fernandez lavas reveal variable contributions from a high-$^3He/^4He$ mantle plume

Thi B. Truong[1], Paterno R. Castillo*, David R. Hilton, James M.D. Day

Scripps Institution of Oceanography, University of California, San Diego, La Jolla, CA 92093-0212, USA

ARTICLE INFO

Editor: Catherine Chauvel

Keywords:
Juan Fernandez
$^3He/^4He$
Mantle plume
Sr-Nd-Pb isotopes
Isotope decoupling
FOZO

ABSTRACT

The Juan Fernandez Islands in the southeastern Pacific are an atypical linear volcanic chain that exhibits a considerable range in $^3He/^4He$ ratios (8 to 18 R_A, where R_A is the $^3He/^4He$ ratio of air), but limited ranges of $^{87}Sr/^{86}Sr$ and $^{143}Nd/^{144}Nd$. Here we report new trace element abundance data and Sr-Nd-Pb isotope data for mafic lavas previously analyzed for their $^3He/^4He$ and He contents from the two main islands of Robinson Crusoe and Alexander Selkirk. Lavas from these islands have been previously grouped based on geochemical and petrological classification into Group I and III basalts, and Group II basanites. In general, samples have overlapping Sr-Nd-Pb isotope compositions that suggest a common, albeit slightly heterogeneous mantle source. In detail, the Group I and III tholeiitic and alkalic basalts have nearly identical incompatible trace element patterns, whereas the Group II basanites show elevated incompatible trace element abundances. Major and incompatible trace element modeling indicates that Group III basalts ($^3He/^4He$ = 7.8–9.5 R_A) from younger Alexander Selkirk Island were produced by the highest degree of partial melting (> 10%) of a common mantle source, followed by Group I basalts (13.6–18.0 R_A) and Group II basanites (11.2–12.5 R_A) from older Robinson Crusoe Island. The $^{206}Pb/^{204}Pb$ of Group I basalts and Group II basanites are slightly more radiogenic and limited in range (19.163 to 19.292) compared with those of Group III (18.939 to 19.221). The Group I and II lavas from Robinson Crusoe are consistent with an origin from the so-called focus zone (FOZO) mantle component, whereas the Alexander Selkirk basalts additionally contain contributions from a less-enriched or relatively depleted mantle component. Juan Fernandez lavas reveal limited ranges of Sr-Nd-Pb isotopes but variable $^3He/^4He$ as their parental magmas originated mainly from the FOZO component with high $^3He/^4He$ (> 9 R_A) and variably polluted with a depleted component with lower $^3He/^4He$ (ca. 8 R_A). Contributions from high-$^3He/^4He$ mantle sources to ocean island basalts can therefore vary both spatially and temporally, over meter to kilometer lengths and hundred to million-year time scales, and may not be strongly correlated to radiogenic lithophile isotope systematics.

1. Introduction

Ocean island basalts (OIB) exhibit a range of radiogenic isotope variability (e.g., $^{87}Sr/^{86}Sr$, $^{143}Nd/^{144}Nd$, $^{206}Pb/^{204}Pb$) that provides invaluable information on the long-term composition of OIB mantle sources (Gast et al., 1964; Kay et al., 1970). These traits have led to wide acceptance that OIB come from heterogeneous, variably enriched and ancient mantle sources. In the hotspot or plume hypothesis, which posits intraplate volcanoes are formed by magmas erupted through oceanic plates moving over pseudo-stationary heat sources originating within the mantle (Wilson, 1963; Morgan, 1972), the OIB mantle sources are comprised of 'reservoirs' containing high μ (HIMU), enriched mantle 1 (EM1) and enriched mantle 2 (EM2) end-components (Zindler and Hart, 1986; Hart et al., 1992). Together with the geochemically depleted mid-ocean ridge basalt (MORB) mantle (DMM) end-component, they define a tetrahedron in three-dimensional Sr-Nd-Pb isotopic space that contains a focus zone (FOZO), where the components appear to converge (Hart et al., 1992; Hauri et al., 1994). The alternative non-plume proposal, on the other hand, suggests that the heterogeneous composition of OIB reflects variable, but generally lower degrees of partial melting of the ubiquitously heterogeneous upper mantle (Foulger, 2011 and references therein).

Noble gases are key tracers of mantle geochemistry because they are chemically inert, are highly incompatible and thus partition into the melt phase, and display wide and diagnostic variations in their isotope characteristics (Hilton and Porcelli, 2014). Among the noble gases, He isotopic analyses of MORB and OIB are most abundant with early reports of high-$^3He/^4He$ values (> 8 ± 1 R_A, the nominal MORB value;

* Corresponding author.
E-mail address: pcastillo@ucsd.edu (P.R. Castillo).
[1] Present address: College of Earth, Ocean, and Atmospheric Sciences, Oregon State University, Corvallis, OR, 97331, USA.

https://doi.org/10.1016/j.chemgeo.2017.11.024
Received 31 May 2017; Received in revised form 7 November 2017; Accepted 20 November 2017
Available online 26 November 2017
0009-2541/

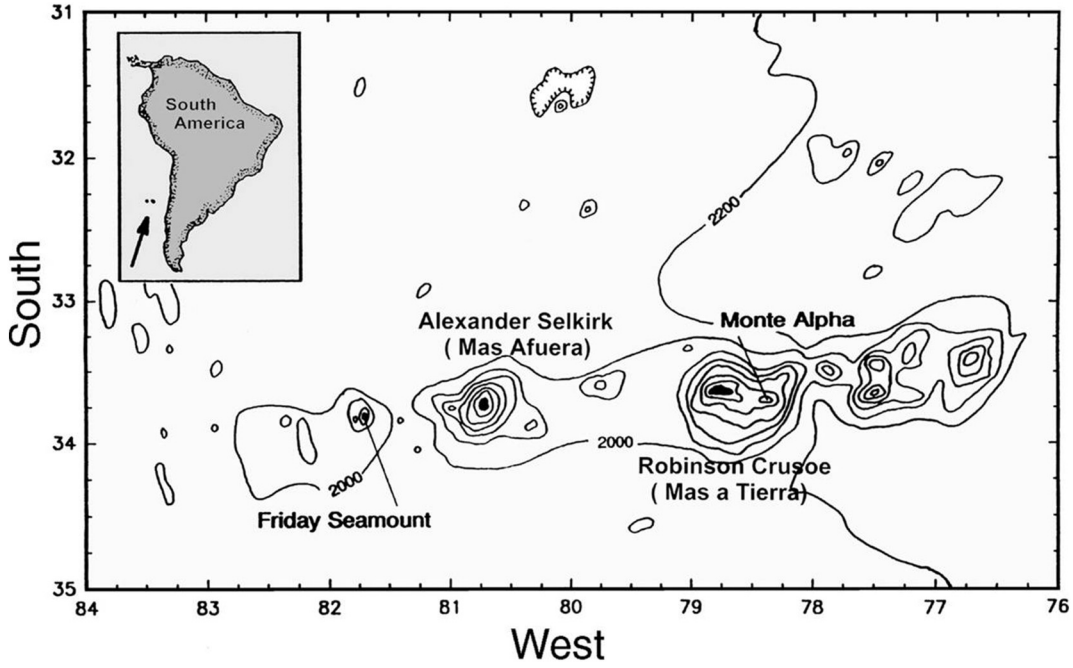

Fig. 1. Bathymetric map of Juan Fernandez Islands from Farley et al. (1993).

R_A = value relative to air $^3He/^4He$) in Hawaiian lavas used to bolster the deep mantle or plume origin of OIB (Craig and Lupton, 1976). In this model, portions of the lower mantle have not yet undergone significant mixing with, and/or may be relatively undegassed relative to, the upper mantle so they retain a greater proportion of their primordial volatile content (Craig and Lupton, 1981). Helium and Sr-Nd-Pb isotopes can correlate in OIB (e.g., Farley et al., 1992; Hanan and Graham, 1996; Hilton et al., 1999). Consequently, the plume model invokes a common, high-$^3He/^4He$ deep mantle component that has been termed PHEM (primitive helium mantle - Farley et al., 1992), "C" (common - Hanan and Graham, 1996) or the aforementioned FOZO (Hart et al., 1992); these terms differ only in the details of Sr, Nd and Pb isotopes, if at all (Hofmann, 2014). Thus, OIB with high-$^3He/^4He$ offer unique insights into the magma source and evolution of linear volcanic chains.

The east-west trending Juan Fernandez linear volcanic chain in the southeastern Pacific (Fig. 1) is an important case study for helium isotopic variations in OIB because its lavas span a range in $^3He/^4He$ values between 7.8 and 18.0 R_A (Farley et al., 1993). This variation spans the typical ratio of MORB (8 ± 1 R_A; Graham, 2002) into the range of the higher ratios measured for some intraplate lavas (> 9 and up to ca. 50 R_A; Stuart et al., 2003). As with models for Hawaiian magmatic evolution, an early popular explanation is that a stationary mantle plume formed the Juan Fernandez linear volcanoes because of the eastward movement of the Nazca plate over the Juan Fernandez plume, creating new volcanoes in the west and cutting off supply to older ones in the east (Baker et al., 1987; Farley et al., 1993).

Results of these early investigations, however, also showed fairly homogeneous Sr-Nd isotopic ratios of Juan Fernandez lavas (Gerlach et al., 1986; Farley et al., 1993). This means that despite their large range of He isotopic variation, Juan Fernandez lavas show limited to no correlation between He and Sr-Nd isotope ratios. Similar to other high-$^3He/^4He$ OIB (e.g., from Heard, Samoa, Iceland, and Hawaii), however, the highest $^3He/^4He$ values of Juan Fernandez lavas generally converge at the PHEM, C or FOZO mantle component (e.g., Farley et al., 1992; Hanan and Graham, 1996; Hilton et al., 1999; Castillo et al., 2007). As FOZO is the convergence of almost all OIB, it is perhaps volumetrically and compositionally the most dominant component of mantle plumes (Castillo, 2015, 2017) and, thus, needs to be better understood. On the other hand, Natland (2003) argued that the He contents of olivine crystals in Juan Fernandez lavas were not derived from mantle plumes but were instead indicative of volatiles that permeated shallow magma reservoirs and subsequently became trapped in crystallizing olivine. This notion, together with the atypical lack of $^3He/^4He$ correlation with Sr-Nd isotopes, had been used as a major argument in favor of the plume counter-proposal that OIB composition is not definitive of distinct mantle end-components and, thus, is not directly connected to deep mantle plumes (Foulger, 2011 and references therein).

In this study, we further examine the petrology and geochemistry of Juan Fernandez lavas to better constrain their petrogenesis and the nature of their mantle source. Our new trace element and Sr-Nd-Pb isotopic analyses, combined with available He and Sr-Nd isotopes (Farley et al., 1993), indicate that sampling through variable degrees of partial melting and inherent heterogeneity of the nominally high-$^3He/^4He$ mantle plume source (or FOZO) can explain the distinct lava groups of Juan Fernandez lavas despite their limited Sr-Nd-Pb isotope variation.

2. Geologic background and samples analyzed

The island and seamount chain comprising the Juan Fernandez linear volcanoes is located at latitude 34°S in the southeastern Pacific, some 660 km west of the Chilean coast (Fig. 1). The chain spans about 800 km on the ca. 22 to 37 Ma old Nazca Plate (Baker et al., 1987; Corvalan, 1981; Gripp and Gordon, 2002; Rodrigo and Lara, 2014). The Juan Fernandez Islands consist of two main islands 180 km apart, Robinson (R.) Crusoe (also known as Mas a Tierra, closer to the land) and Alexander (A.) Selkirk (Mas Afuera, away from the land), and a small island located southwest of R. Crusoe, Santa Clara (Baker et al., 1987; Farley et al., 1993; Devey et al., 2000; Rodrigo and Lara, 2014). Two prominent seamounts, Friday and Domingo, lie west of A. Selkirk.

The stratigraphy of the islands is poorly known, but radiometric (K-Ar) ages for R. Crusoe lavas range from 5.8 to 3.1 Ma whereas those for A. Selkirk range from 2.5 to 0.85 Ma (Booker et al., 1967; Stuessy et al., 1984; Baker et al., 1987). Dredged fresh basalts suggest Friday and Domingo seamounts are younger than A. Selkirk (Farley et al., 1993). Devey et al. (2000) also noted that the larger Friday Seamount appears morphologically evolved with evidence of volcanic activity over a

broad area and is likely to be older than Domingo that lies to the west. Moreover, Domingo Seamount has less sediment cover (Devey et al., 2000). The ages of island samples as well as observational data for the seamounts are consistent with the proposed eastward age-progression of volcanism in the Juan Fernandez volcanic chain (Farley et al., 1993; Devey et al., 2000; Gripp and Gordon, 2002).

We focused on the suite of samples from R. Crusoe and A. Selkirk that were collected during Leg 1 of the Scripps Institution of Oceanography (SIO) HYDROS expedition aboard R/V Melville in 1988. Major and select trace element compositions, lithologic and field descriptions as well as He-Sr-Nd isotopic data have been reported previously (Farley, 1991; Farley et al., 1993). Olivine grains from some of the samples have also been analyzed for oxygen isotopes (Eiler et al., 1997). Based on normative mineralogy, the samples consist of olivine tholeiites, alkali basalts and basanites. Moreover, the samples had previously been classified into four groups namely I, II, III, and IV by Farley and co-workers (Farley, 1991; Farley et al., 1993). Groups I and II consist of basalts and basanites, respectively, from R. Crusoe whereas Group III consists of A. Selkirk basalts, which are lithologically and chemically similar to Group I basalts. The few Group IV lavas consist of Friday Seamount alkali basalts that are reported to be like R. Crusoe and A. Selkirk basalts; they are not included in this investigation.

Baker et al. (1987) initially classified eight groups of Juan Fernandez lavas based on geographic distribution of rock units, but later adopted two broad geochemical groups for R. Crusoe: central and peripheral. Central group consists of picritic basalts, aphyric alkalic basalts and quartz tholeiites whereas peripheral group includes olivine tholeiites, alkali basalts and basanites. The recent and more detailed work on R. Crusoe by Reyes et al. (2017), however, favors a central structure scheme with a gently dipping shield sequence cross-cut by dyke complexes (shield unit) that is separated by an unconformity from the overlying lavas and pyroclastic beds erupted from several small and isolated vents (rejuvenated unit). Significantly, the basanites occur as dikes and as parasitic cones along the southwest peninsula (Gerlach et al., 1986). Group I basalts and the lithologically and compositionally akin Group III basalts from A. Selkirk investigated here belong mainly to the shield unit whereas Group II basanites are post-shield lavas that belong to the rejuvenated unit of Reyes et al. (2017).

3. Analytical methods

Seventeen lavas were analyzed for their trace element (Rb, Sr, Y, Ba, Pb, Th, rare earth elements (REE), and high field-strength elements (HFSE) Nb, Ta, Zr, and Hf) and Pb isotopic compositions. Strontium and Nd isotopes were also analyzed for one sample (PF-21) to replicate the findings by Farley et al. (1993), and for three samples (PF-3, MF-16, MF-6) that had not been analyzed previously. Lead isotopes were determined for all 17 lavas. All analyses were performed on whole-rock samples. Neodymium isotopes of olivine separates from five samples (MF-3, PF-21, PF-5, PF-10, PIN-8) spanning the range of $^{3}He/^{4}He$ ratios from 7.8 to 18.0 R_A were also analyzed.

For the analyses, the fresh interior portions of the samples were crushed to cm-size fragments, ultrasonically cleaned in a ca. 5% HNO_3 solution to cleanse any contamination such as metals and extra powder from crushing, and dried in an oven at ca. 110 °C. Once dried, the fragments were powdered in an alumina ceramic shatter box. Trace elements were determined on unleached powders by inductively-coupled plasma mass spectrometry (ICP-MS) using a *ThermoQuest Element 2* instrument. Strontium, Nd and Pb isotopes were also analyzed on unleached powders through thermal ionization mass spectrometry (TIMS) using a *Micromass VG 54* instrument. The samples were not leached because most of them are relatively unaltered, as evidenced by the presence of groundmass and phenocrystic olivine. More importantly, we want to directly combine our analyses with previous major-trace element and Sr-Nd isotope data collected from unleached samples by Farley and co-workers (Farley, 1991; Farley et al., 1993). The sample digestion procedure used for the ICP-MS and TIMS analyses is like that described in Janney and Castillo (1996). For trace element analysis, about 20 mg of sample powder was dissolved in a clean Teflon beaker using a doubly-distilled HF:HNO_3 (2:1) mixture, dried over a hotplate, and evaporated twice in concentrated HNO_3. The dissolved sample was diluted ca. 4000× with a 1% HNO_3 solution containing 1 ppb ^{115}In as an internal standard to correct for signal run intensity variation and instrumental drift.

For Pb, Sr and Nd isotope analysis, each sample was dissolved as above and then re-dissolved in 4.5 N HCl, dried, then dissolved again in 2.5 N HBr, dried, and finally passed through a cation column in a HBr medium to collect Pb. The left-over sample solution from the Pb column was dried and loaded into a primary cation column in a chloride medium to collect Sr and REE. Finally, the REE cut was passed through an ion exchange column in an alpha HIBA (alpha-hydroxyisobutyric) acid medium to collect Nd (Janney and Castillo, 1996; Castillo et al., 2007).

Olivine separates analyzed for Nd isotopes were hand-picked under a binocular microscope from aliquots of the cm-sized fragments of whole rock samples prepared by Farley (1991). Approximately 70 mg of separates were then ultrasonically cleaned with a 1% HNO_3 solution and dried in an oven at ca. 110 °C prior to dissolution. The olivine separates were dissolved in the same way as the whole rock powders. The separates were not crushed prior to dissolution. Neodymium was separated from the olivine solution as described above and analyzed through TIMS to directly compare their $^{143}Nd/^{144}Nd$ and $^{3}He/^{4}He$ compositions. Despite the low concentration of Nd in olivine, $^{143}Nd/^{144}Nd$ was measured on the separates. The measurements, however, took longer and the ratios typically have larger uncertainties (2σ instrumental error up to ± 32 – Table 1) compared to those of the whole rocks.

Additional details of the analyses plus analytical uncertainties are reported as footnotes to Table 1.

4. Results

4.1. Trace elements

The trace element compositions of the samples are presented in Table 1. Their Ba/Zr ratios are consistent with the subdivision of the samples into Group I (average Ba/Zr = 0.87), Group II (average Ba/Zr = 1.67) and Group III (average Ba/Zr = 0.59; Farley et al., 1993) (Fig. 2A). The only exception is sample PV-2, which Farley and co-workers designated as basanite based on its ca. 5% normative nepheline, but new results show that its Ba/Zr (1.05) as well as other geochemical characteristics plot closer to Group I basalts. We re-classify this sample as Group I basanitoid. Zirconium also correlates well with Nb and the overall Nb/Zr range (0.11–0.27) is consistent with high ratios (> 0.1) of OIB (Fig. 2B). Group II basalts have the highest Nb and Zr contents (> 58 and > 228 ppm, respectively) whereas Groups I and III have similarly lower values (< 42 ppm Nb, < 253 ppm Zr). Group I has lower Nb for given Zr values than Group II.

Juan Fernandez lavas have light-REE enriched primitive mantle-normalized patterns, also typical of OIB (Fig. 3A). Most of the samples plot within the range of previous REE analyses by Baker et al. (1987) and display the same three groups as proposed by Farley and co-workers. Samples from both islands have roughly similar average light- to medium-REE slopes, but their average $(La/Sm)_N$ values slightly differ (Group III = 2.0 ± 0.3, Group I = 1.9 ± 0.3 and Group II = 3.4 ± 0.3). Moreover, the normalized concentration patterns show that Group III is less fractionated (average $(La/Yb)_N$ = 9.0) than both Groups I and II (Group II average $(La/Yb)_N$ = 20.2). Most samples reveal a slightly positive Eu concentration anomaly, or Eu enrichment relative to adjacent trace elements in normalized plots, with Group III showing the greatest anomaly whereas Group I has the smallest.

The primitive mantle-normalized spidergram shows the entire lava

Table 1
Trace element and isotope data for Juan Fernandez lavas.

Sample	PV-2	PV-4	PF-3	PF-5	PF-10	PIN-12
Group	I	I	I	I	I	I
Rock type[a]	A.B.	O.T.	A.B.	A.B.	O.T.	O.T.
Rb (ppm)	8.42	14.9	6.73	20.9	15.6	6.00
Ba	208	169	164	236	177	100
Nb	33.9	33.9	29.3	41.9	34.1	22.5
Sr	584	388	412	540	425	317
Zr	198	205	183	242	180	156
Y	15.9	21.4	17.5	20.0	20.2	16.3
La	8.47	20.08	9.78	15.91	14.31	9.1
Ce	19.65	42.86	21.7	34.77	30.01	20.2
Pr	2.91	5.67	3.07	4.57	4.21	2.75
Nd	13.08	23.01	12.86	18.79	17.83	11.25
Sm	3.6	5.47	3.5	4.59	4.48	2.93
Eu	1.79	1.92	1.59	1.91	1.81	1.19
Tb	0.52	0.74	0.52	0.64	0.69	0.45
Dy	4.91	3.68	3.2	3.68	4.11	2.85
Ho	0.6	0.8	0.62	0.68	0.75	0.55
Er	1.61	2.1	1.68	1.79	2.01	1.48
Yb	1.24	1.57	1.32	1.3	1.58	1.09
Lu	0.18	0.22	0.19	0.19	0.22	0.16
Hf	4.4	4.48	4.12	5.16	4.11	3.52
Ta	2.11	2.07	1.81	2.41	2.06	1.39
Pb	1.13	1.66	1.25	1.82	1.65	0.80
Th	1.90	2.46	2.19	2.45	1.93	1.40
U	0.59	0.78	0.33	0.93	0.43	0.27
Ba/Zr	1.05	0.82	0.90	0.98	0.98	0.64
Nb/Zr	0.17	0.17	0.16	0.17	0.19	0.14
La/Yb	6.85	12.78	7.39	12.22	9.04	8.36
$^{87}Sr/^{86}Sr$[b]	*0.703660*	*0.703460*	0.703698 (12)	*0.703410*	*0.703640*	*0.703510*
$^{143}Nd/^{144}Nd$[b]	*0.512856*	*0.512876*	0.512835 (5)	*0.512886*	*0.512876*	*0.512836*
$^{143}Nd/^{144}Nd_{olivine}$				0.512808 (14)	0.512827 (9)	
$^{206}Pb/^{204}Pb$	19.194	19.258	19.292	19.166	19.224	19.189
$^{207}Pb/^{204}Pb$	15.666	15.675	15.669	15.647	15.678	15.653
$^{208}Pb/^{204}Pb$	39.161	39.276	39.291	39.099	39.310	39.184

Sample	PIN-8	PF-16	PV-1	PF-21	PF-17	MF-C4
Group	I	II	II	II	II	III
Rock type[a]	O.T.	BSN	BSN	BSN	BSN	O.T.
Rb (ppm)	2.46	38.1	57.5	54.8	44.2	19.9
Ba	104	403	616	599	559	150
Nb	20.5	57.7	99.6	96.8	90.1	28.4
Sr	319	661	932	862	825	381
Zr	141	228	383	357	339	281
Y	14.7	28.9	37.2	31.8	29.50	28.9
La	7.40	32.99	56.52	50.64	44.09	17.87
Ce	16.55	63.98	107.55	97.44	85.42	35.38
Pr	2.42	8.15	13.56	11.78	11.2	5
Nd	10.78	31.15	48.96	41.73	41.39	20.82
Sm	3.06	6.87	9.8	8.5	8.59	5.48
Eu	1.29	2.5	3.43	2.96	3	2.4
Tb	0.47	0.94	1.3	1.12	1.13	0.82
Dy	3.2	4.36	5.57	5.64	6.78	5.18
Ho	0.56	1.01	1.3	1.07	1.08	0.99
Er	1.52	2.78	3.65	2.81	2.81	2.57
Yb	1.15	2.08	2.9	2.09	2.1	1.92
Lu	0.16	0.31	0.42	0.3	0.29	0.28
Hf	3.31	4.79	7.56	6.93	6.66	6.08
Ta	1.33	3.29	5.64	5.27	4.98	1.71
Pb	0.75	2.68	4.55	3.85	4.27	1.46
Th	1.25	4.75	8.10	7.77	6.61	2.60
U	0.17	1.09	1.89	1.65	1.41	0.66
Ba/Zr	0.74	1.76	1.61	1.68	1.65	0.53
Nb/Zr	0.15	0.25	0.26	0.27	0.27	0.10
La/Yb	6.46	15.86	19.50	24.27	21.01	9.29
$^{87}Sr/^{86}Sr$	*0.703650*	*0.703460*	0.703430 (12)	*0.703510*	*0.703420*	*0.703560*
$^{143}Nd/^{144}Nd$	*0.512856*	*0.512896*	0.512870 (6)	*0.512896*	*0.512876*	*0.512886*
$^{143}Nd/^{144}Nd_{olivine}$	0.512824 (9)			0.512837 (9)		
$^{206}Pb/^{204}Pb$	19.179	19.216	19.163	19.182	19.184	19.177
$^{207}Pb/^{204}Pb$	15.638	15.631	15.656	15.637	15.635	15.657
$^{208}Pb/^{204}Pb$	39.138	39.237	39.315	39.271	39.262	39.197

Sample	MF-3	MF-16	MF-6	MF-S1	MF-C2	BHVO-1
Group	III	III	III	III	III	USGS
Rock type[a]	O.T.	O.T.	O.T.	A.B.	O.T.	Hawaiian basalt
Rb (ppm)	11.5	13.0	12.8	13.2	9.16	10.3
Ba	106	111	110	137	136	133
Nb	17.2	20.6	20.1	23.9	26.0	17.4
Sr	320	391	393	382	360	383
Zr	170	189	184	199	253	176
Y	20.5	18.4	21.1	19.0	16.1	25.5
La	12.17	8.54	10.49	11.94	6.93	15.4
Ce	26.56	18.72	23.23	25.53	15.47	37.4
Pr	3.97	2.78	3.47	3.83	2.24	5.40
Nd	17.12	12.15	15.26	16.01	9.97	24.10
Sm	4.56	3.45	4.26	4.16	3.00	5.95
Eu	1.61	1.49	1.71	1.65	1.94	2.15
Tb	0.69	0.54	0.65	0.59	0.49	1.03
Dy	4.34	3.39	4.32	3.52	3.73	5.20
Ho	0.78	0.68	0.79	0.67	0.63	0.94
Er	2.08	1.9	2.12	1.71	1.79	2.30
Yb	1.53	1.45	1.6	1.32	1.46	1.98
Lu	0.22	0.22	0.23	0.19	0.21	0.28
Hf	3.87	4.33	4.17	4.42	5.66	4.58
Ta	1.08	1.28	1.25	1.48	1.63	1.18
Pb	0.90	2.76	0.98	1.10	1.09	2.47
Th	1.50	1.34	1.29	1.61	2.12	0.98
U	0.39	0.38	0.35	0.41	0.45	0.43
Ba/Zr	0.63	0.59	0.60	0.69	0.54	0.76
Nb/Zr	0.10	0.11	0.11	0.12	0.10	0.10
La/Yb	7.95	5.87	6.55	9.06	4.76	7.78
$^{87}Sr/^{86}Sr$	*0.703560*	0.703614 (11)	0.703601 (12)	*0.703670*	*0.703570*	
$^{143}Nd/^{144}Nd$	*0.512906*	0.512880 (5)	0.512869 (14)	*0.512886*	*0.512896*	
$^{143}Nd/^{144}Nd_{olivine}$	0.512886 (32)					
$^{206}Pb/^{204}Pb$	18.939	19.221	19.170	19.081	19.158	
$^{207}Pb/^{204}Pb$	15.632	15.684	15.649	15.636	15.652	
$^{208}Pb/^{204}Pb$	38.893	39.138	39.078	39.068	39.188	

Reproducibility of the trace element analyses was better than 5% based on repeated analyses of rock standards analyzed as unknowns. The accuracy of the standard is within 10% of the suggested values (BHVO-1, $n = 33$), but generally better than ± 5% for rare earth elements (REEs). Strontium, Nd and Pb isotope ratios were analyzed using a 9-collector, Micromass Sector 54 thermal ionization mass spectrometer (TIMS). Total procedural blanks are 35 pg for Sr, 10 pg for Nd and 60 pg for Pb. Strontium isotopic ratios were fractionation-corrected to $^{86}Sr/^{88}Sr = 0.1194$ and are reported relative to $^{87}Sr/^{86}Sr = 0.710254 \pm 0.000018$ ($n = 22$) for NBS 987 during the period of analysis. Neodymium isotopic ratios were measured in oxide form, fractionation corrected to $^{146}NdO/^{144}NdO = 0.72225$ ($^{146}Nd/^{144}Nd = 0.7219$) and are reported relative to $^{143}Nd/^{144}Nd = 0.511856 \pm 0.000016$ ($n = 19$) for the La Jolla Nd Standard during the period of analysis. Numbers in parentheses after $^{87}Sr/^{86}Sr$ and $^{143}Nd/^{144}Nd$ are instrumental (2σ) errors and refer to the last significant figures. Strontium and Nd isotope values from Farley et al. (1993) have been normalized to the measured standard values ($^{87}Sr/^{86}Sr = 0.710254$; $^{143}Nd/^{144}Nd = 0.511856$). Lead isotopic ratios were analyzed using the double-spike method to correct for mass fractionation during analyses; separate measurements of spiked and unspiked samples were made on different aliquots from the same dissolution. The SBL-74 ^{207}Pb–^{204}Pb double-spike from the University of Southampton was used. During the analysis period, the method produced the following results for NBS 981: $^{206}Pb/^{204}Pb = 16.9300 \pm 0.0020$, $^{207}Pb/^{204}Pb = 15.4896 \pm 0.0027$ and $^{208}Pb/^{204}Pb = 36.6999 \pm 0.0086$ ($n = 11$). 2σ precisions for individual runs are better than these.

[a] BSN = basanite; A.B. = alkali basalt; O.T. = olivine tholeiite.

[b] Values in italics are from Farley et al. (1993).

suite exhibits sub-parallel patterns that are enriched in highly incompatible elements, also typical of OIB (Fig. 3B). Groups I and III again have nearly identical concentration patterns whereas Group II is distinctively more enriched in highly incompatible elements (e.g., Ba and Th up to ca. 90 × primitive mantle), consistent with previous results (Baker et al., 1987; Farley et al., 1993). All groups also display positive Nb and Ta concentration anomalies. Groups I and III basalts likewise display a positive Ti anomaly but Group II does not. In other words, the bulk of Juan Fernandez lavas exhibit enrichment in Ti, Ta and Nb, or the so-called positive 'TITAN' anomalies, which are pervasive features of OIB (Jackson et al., 2008; Peters and Day, 2014).

4.2. Strontium, neodymium and lead isotopes

The Sr, Nd and Pb isotopic compositions of Juan Fernandez lavas are presented in Table 1 and shown graphically in Figs. 4 and 5. Our new and existing analyses by Farley et al. (1993) indeed show limited variations in both $^{87}Sr/^{86}Sr$ (0.70341–0.70370) and $^{143}Nd/^{144}Nd$ (0.51284–0.51291) values (Farley, 1991), but on average are slightly more depleted (lower $^{87}Sr/^{86}Sr$, higher $^{143}Nd/^{144}Nd$) than the analyses of Gerlach et al. (1986; Fig. 4). In detail, Group I samples span the entire range of $^{87}Sr/^{86}Sr$ values although, on average, Group II has the lowest (< 0.70351) and Group III has intermediate (0.70356–0.70367) values. Group I also has the largest range of $^{143}Nd/^{144}Nd$ ratios, but the lowest average value (0.51286). Group II has a moderate range of $^{143}Nd/^{144}Nd$ (0.52187–0.51290) whereas Group III has the highest $^{143}Nd/^{144}Nd$ ratios (up to 0.51291). Overall, Group I is relatively the most isotopically heterogeneous in terms of Sr and Nd isotopic composition; Group II completely overlaps its most depleted (low $^{87}Sr/^{86}Sr$ and high $^{143}Nd/^{144}Nd$) end. Group III is relatively homogeneous and has higher $^{143}Nd/^{144}Nd$ for given $^{87}Sr/^{86}Sr$ than Groups I and II.

Also shown in Table 1 are the Nd isotopic compositions of five olivine separates from at least one sample from each lava group that spans the range of $^{3}He/^{4}He$ (generally from 8 to 18 R_A). The $^{143}Nd/^{144}Nd$ values measured on three olivine separates (PIN-8, MF-3, PF-10) are similar within the analytical uncertainties (± 0.000016 for each) of respective whole rock values whereas the other two (PF-5, PF-21) are outside the analytical uncertainties. The latter two have slightly lower $^{143}Nd/^{144}Nd$ than the whole rock values.

The new $^{206}Pb/^{204}Pb$, $^{207}Pb/^{204}Pb$, and $^{208}Pb/^{204}Pb$ values for Juan Fernandez lavas overlap with previous analyses of Gerlach et al. (1986; Fig. 5). As a whole, however, they are slightly though systematically higher in $^{207}Pb/^{204}Pb$, and $^{208}Pb/^{204}Pb$ for a given $^{206}Pb/^{204}Pb$ than the latter data set, although are still relatively limited in composition. In detail, our Groups I and II samples completely overlap in $^{206}Pb/^{204}Pb$ and $^{208}Pb/^{204}Pb$ values, like their Sr and Nd isotopes, and are more

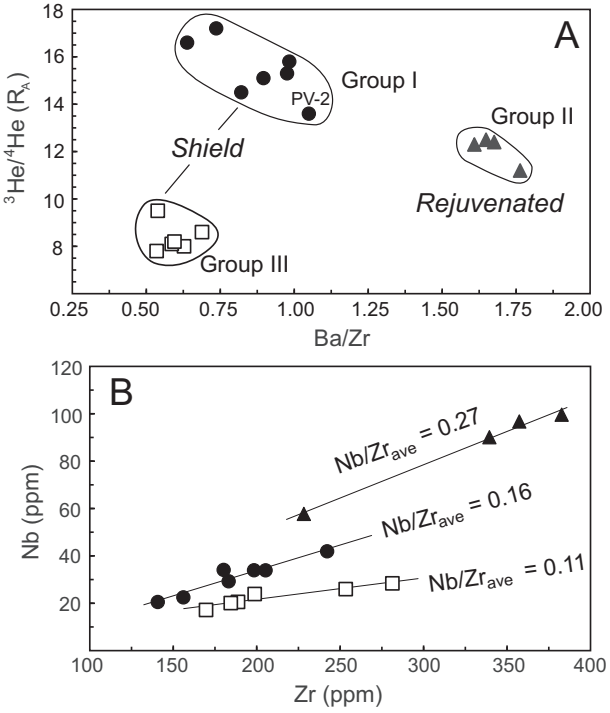

Fig. 2. (A) $^3He/^4He$ (R_A) versus Ba/Zr diagram for lavas from Juan Fernandez Islands (slightly modified after Fig. 4A of Farley et al., 1993), showing Groups I, II and III lavas. (B) Nb (ppm) versus Zr (ppm) diagram. PV-2 is a Group I basanitoid.

radiogenic than Group III. There is no apparent distinction among the groups in terms of $^{207}Pb/^{204}Pb$ ratios. Juan Fernandez Pb isotopic arrays lay parallel and above the northern hemisphere reference line (NHRL) and do not trend toward the Pacific DMM source.

5. Discussion

Despite limited Sr-Nd-Pb isotopic variation (Figs. 4 and 5), the new trace element data show large variation and support the previous chemical classification scheme for the R. Crusoe and A. Selkirk lavas (Figs. 2 and 3). Moreover, major element data are also variable and show that Juan Fernandez basalt to trachyte lavas define coherent trends or liquid lines of descent in most MgO variation diagrams. These trends indicate that fractional crystallization of individual batches of parental basaltic magmas erupted at different times in the two islands is mainly responsible for some of the compositional variations within and among the lava groups (Truong, 2015). On the other hand, the trace element variations of the lavas (Fig. 2) plus the variable, though limited Sr, Nd and Pb isotopic variations (Figs. 4 and 5) suggest that the parental basaltic magmas of Juan Fernandez lavas originate from a mantle source with a slightly heterogeneous composition (see also Farley et al., 1993). To a first order the major and trace element variations of the parental magmas of Juan Fernandez lava groups can be ascribed to partial melting of a common, slightly heterogeneous, mantle source.

5.1. Elemental variations as a function of partial melting

Our Juan Fernandez lava suite is biased toward picritic compositions (> 13.5 wt% MgO) due to preferential sampling of olivine-accumulative rocks for He isotope work and, thus, does not represent the liquidus composition of primary magmas (Farley, 1991; Farley et al., 1993; Baker et al., 1987). Qualitatively, Group II has the highest Na_2O for given MgO values among the basalts and also has slightly higher FeO* for a given MgO than Group I (Truong, 2015). These compositional features generally suggest that Group II basanites were most likely produced by a relatively smaller degree of partial melting at high

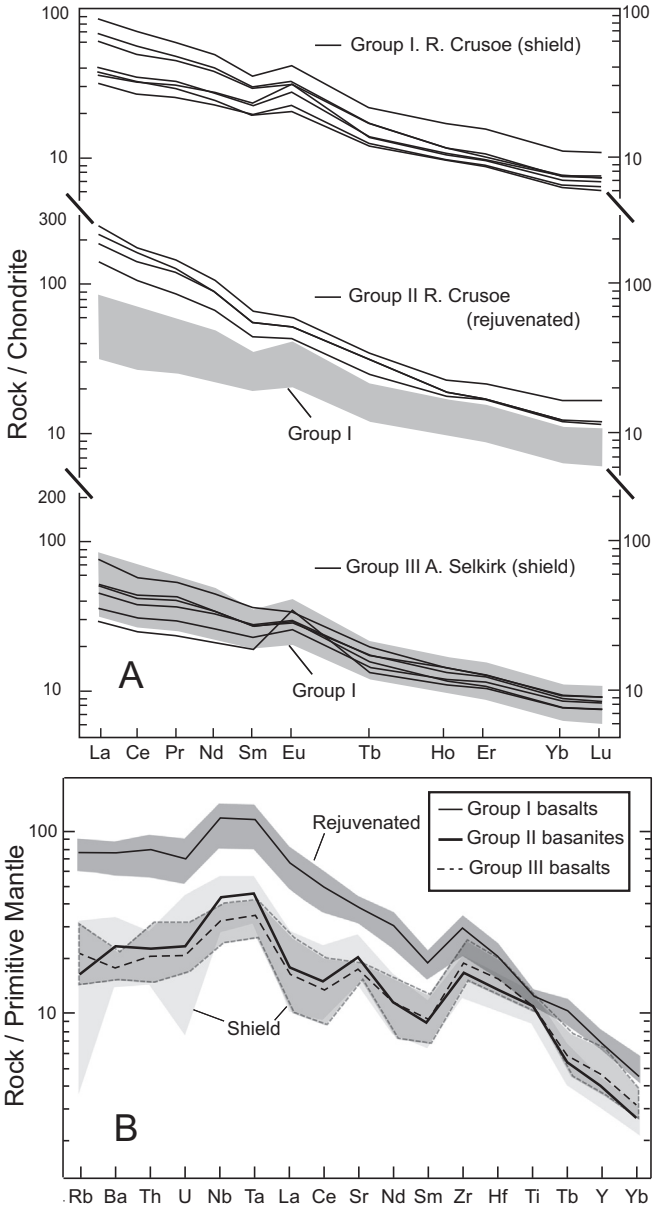

Fig. 3. (A) Chondrite-normalized REE concentration patterns of Juan Fernandez lavas. Shaded region is the range of values for group I olivine tholeiites. (B) Primitive mantle-normalized incompatible trace element concentration patterns. Regions with different shades of gray represent ranges of Groups I and III lavas. Average concentrations are shown. Data from Farley et al. (1993) are included and normalizing values are from Sun and McDonough (1989).

pressure (e.g., Klein and Langmuir, 1987; Niu and O'Hara, 2008). On the other hand, Group I on average has a large range of Na_2O and includes the lowest Na_2O plus low FeO*, whereas Group III has uniform and intermediate Na_2O and highest FeO*. These characteristics suggest Groups I and III were produced by moderate degrees of partial melting at low to moderate pressures (e.g., Klein and Langmuir, 1987; Niu and O'Hara, 2008).

Group II basalts are the most enriched in highly incompatible trace elements and Group I is slightly more enriched than Group III. The incompatible trace element variations of Juan Fernandez lavas when plotted in the process identification diagrams of Allègre and Minster (1978; see also Feigenson et al., 1983) show that Group II basanites were produced by limited degrees of partial melting of the common source whereas Group I and III basalts were produced by higher degrees of partial melting (Fig. 6A and B). This is consistent with the steep REE

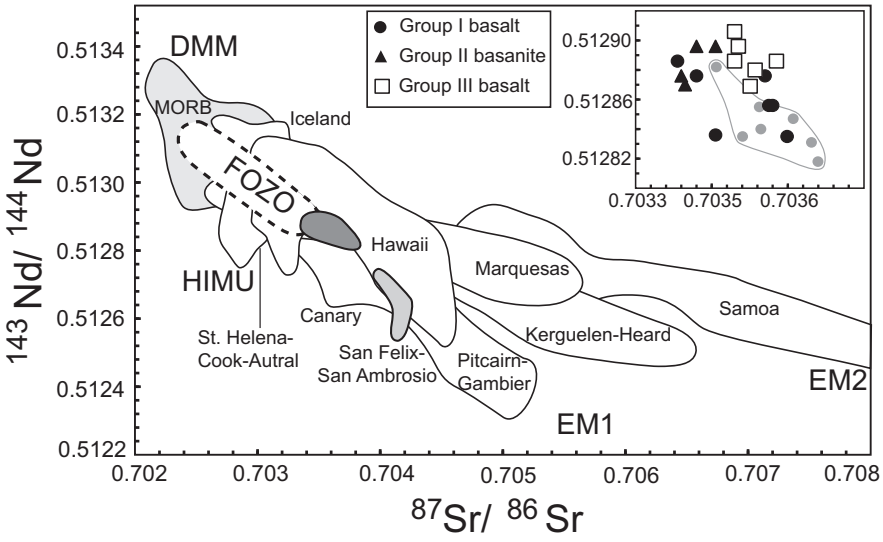

Fig. 4. $^{143}Nd/^{144}Nd$ versus $^{87}Sr/^{86}Sr$ diagram for Juan Fernandez lavas relative to some OIB from the GEOROC database (http://georoc.mpchmainz.gwdg.de/georoc/). Inset shows details of the $^{143}Nd/^{144}Nd$ versus $^{87}Sr/^{86}Sr$ for Juan Fernandez (gray field in the inset encloses data from Gerlach et al., 1986). The expanded FOZO field includes the 'FOZO' and 'C' fields of Hofmann (1997) and Stracke (2012); see text for additional discussion.

patterns and greatest enrichments in highly incompatible elements of Group II (Figs. 3 and 4). Moreover, Group III appears to have undergone a slightly larger degree of partial melting than Group I. The plots also show that a large part of the trace element variations of Group II, even though these are all high MgO (> 11 wt%) basanites, fall to the right of the batch partial melting curve, indicating enrichment due to variable degrees of fractional crystallization or olivine accumulation. The latter process most probably occurred during transit from the deep mantle to the surface as geothermobarometric and textural data indicate polybaric crystallization at a wide range of pressures (Reyes et al., 2017). Fractional crystallization is also consistent with the distinct inverse correlation between MgO and Nb in the basanites in contrast to the nearly constant Nb contents for the range of MgO in Groups I and III basalts (Truong, 2015). Significantly, a similar difference in incompatible trace element concentrations exist between current Galápagos volcanoes and their apparent track along the Cocos Ridge and this has also been interpreted as due to differences in extent of partial melting of a common, heterogeneous source (Hoernle et al., 2000).

Model calculations using the variation of La/Yb versus Dy/Yb illustrate that Groups I and III basalts can be produced by 5 to > 10%

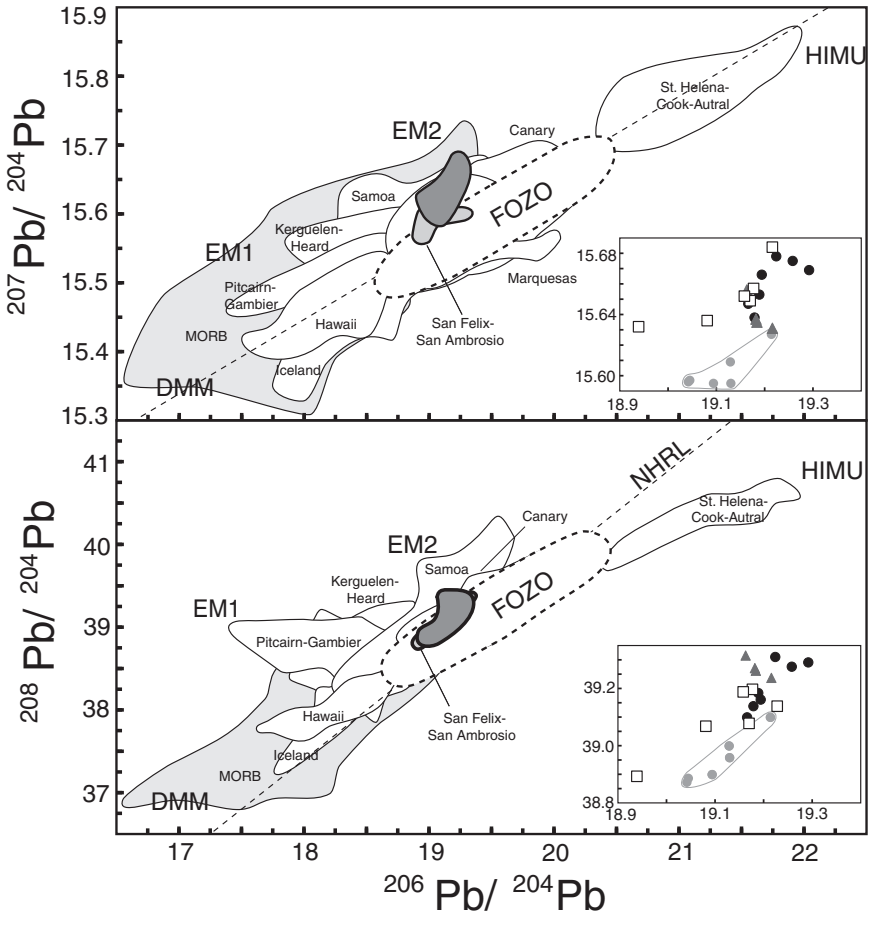

Fig. 5. $^{206}Pb/^{204}Pb$ versus $^{207}Pb/^{204}Pb$ and $^{208}Pb/^{204}Pb$ diagrams for Juan Fernandez lavas from this study and Gerlach et al. (1986). Symbols as in Fig. 4. Insets show details of Juan Fernandez analyses (field in the inset encloses data from Gerlach et al., 1986). Fields for other OIB from the GEOROC database (http://georoc.mpchmainz.gwdg.de/georoc/) are shown for comparison. NHRL is the Northern Hemisphere reference line (Hart, 1984). The locations of the four proposed mantle endmembers DMM, HIMU, EM1, and EM2 are from Zindler and Hart (1986); the expanded fields for FOZO are modified after Stracke (2012).

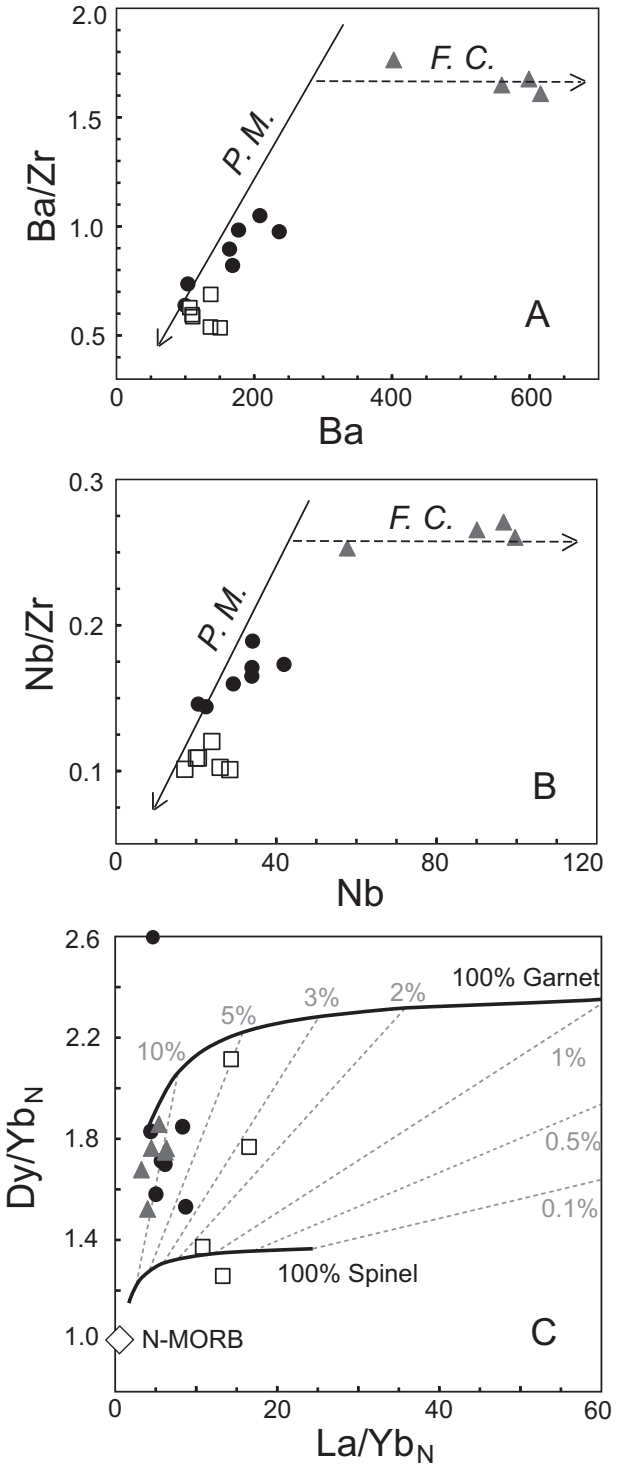

Fig. 6. A. and B., Magmatic process identification diagrams after Allègre and Minster (1978) for Juan Fernandez lavas. Symbols as in Fig. 4. PM represents equilibrium batch partial melting and FC represents fractional crystallization. C. La/Yb versus Dy/Yb for Juan Fernandez lavas. A partial melting model for a primitive mantle source is shown, using the parameters given in Day et al. (2010). Estimates of partial melting are made assuming a primitive mantle source with garnet peridotite starting modal proportions of olivine, orthopyroxene, clinopyroxene, and garnet of 0.598/0.211/0.076/0.115 and a spinel peridotite with olivine, orthopyroxene, clinopyroxene and spinel of 0.578/0.21/0.119/0.033, with appropriate phases melting and partitioning.

polybaric partial melting of a spinel to garnet lherzolite source (Fig. 6C). On average, Group III is produced at higher degrees of partial melting than Group I. On the other hand, Group II basanites have the highest La/Yb and indicate that they can be produced at relatively low degrees (2–6%) of partial melting. Thus, model calculation results are consistent with Group I and III Juan Fernandez lavas being produced by a higher degree of partial melting than Group II basanites.

In summary, the major and trace element variations of Juan Fernandez lavas can be explained through variations of degree and, to a certain extent, pressure (depth) of partial melting of a common, slightly heterogeneous mantle source characterized by a limited Sr, Nd and Pb isotopic variation (Figs. 4 and 5). The geochemistry of Group II can be modeled as the result of a small degree of partial melting (+ fractional crystallization and/or olivine accumulation) whereas those of Groups I and III represent larger degree of partial melting.

5.2. The Sr-Nd-Pb isotopic composition of the mantle source

Despite the clear trace element-$^{3}He/^{4}He$ classification of Juan Fernandez lavas (Fig. 2a), there is limited Sr-Nd-Pb isotopic variation (Figs. 4 and 5). In detail, however, the combined Sr, Nd and Pb isotope data show two slightly different though distinct components in their mantle source (see also Gerlach et al., 1986; Farley et al., 1993). Group I represents the most enriched component, which on average has the lowest $^{143}Nd/^{144}Nd$ and most radiogenic $^{206}Pb/^{204}Pb$ ratios. Although Groups I and II overlap, Group II generally occupies the less radiogenic end of the Group I isotopic range. On the other hand, Group III represents the least enriched component, which on average has the highest $^{43}Nd/^{144}Nd$ and least radiogenic $^{206}Pb/^{204}Pb$ and $^{208}Pb/^{204}Pb$ of the three groups.

From Sr-Nd-Pb isotopic variations, the long-lived radiogenic isotopic ratios of Juan Fernandez indicate a mantle source that is within or approaches the putative FOZO composition (Figs. 4 and 5). The origin of FOZO is controversial (Hart et al., 1992; Hauri et al., 1994; Hilton et al., 1999; Stracke et al., 2005; Hanan and Graham, 1996; Hofmann, 1997; Stracke, 2012; Hofmann, 2014; White, 2015; and references therein). For example, FOZO may be a region in the mantle containing recycled crustal protoliths with continental Pb and located in the transition zone above the 670-km discontinuity (Hanan and Graham, 1996). It may also represent ancient recycled ocean crust and lithosphere that are effectively mixed with the mantle (Day et al., 2010). Alternatively, as the $^{143}Nd/^{144}Nd$ and $^{87}Sr/^{86}Sr$ of FOZO are between bulk silicate Earth (BSE) and DMM (Fig. 4), it may represent the lower, ultramafic portion of previously subducted oceanic slabs (Castillo, 2015, 2016). That is, FOZO could be a representation of the long-term (Ga) time-integrated record of the geochemical depletion of upper mantle with time, from BSE to modern DMM. In terms of Pb isotopes, FOZO is a “young HIMU” that also has a range of radiogenic Pb isotopic ratios between DMM and classic HIMU (Fig. 5) (Vidal, 1992; Thirlwall, 1997; Stracke et al., 2005; Castillo, 2015, 2016). In other words, the variable Sr, Nd and Pb isotopic compositions, as well as the distinctively high and variable $^{3}He/^{4}He$ ratios of FOZO can be a collective, inherent feature of subducted oceanic lithospheric mantle.

In summary, the combined He-Sr-Nd-Pb isotopes indicate that parental magmas of Groups I and II lavas most likely originated from FOZO. Parental magmas of Group III basalts most likely also originated from FOZO but additionally contained a relatively less-enriched or “depleted” component. Notably, Gerlach et al. (1986) suggested a similar, dual mantle source for Juan Fernandez. Their suggestion was deduced from the combined isotopic data for Juan Fernandez plus those of the aforementioned San Felix and San Ambrosio islands (Figs. 5 and 6). Gerlach et al. (1986) showed that these islands define an array representing a mixture of EM1 and classic HIMU end-components. In this study, however, the isotopic data for Juan Fernandez as well as those for San Felix-San Ambrosio islands represent a mixture of a depleted and FOZO (or young HIMU) components.

5.3. Geochemical and volcanologic evolution of Juan Fernandez Islands

Many major geologic features of Juan Fernandez Islands are similar to those of other linear island volcanic chains. For example, the geochemical evolution of Juan Fernandez Islands generally resembles that of Jasper Seamount, which belongs to the Fieberling-Guadalupe Seamount Trail in the eastern Pacific that, in turn, displays many aspects of Hawaiian evolution despite its more limited size (Konter et al., 2009). Fieberling-Guadalupe demonstrates three individual stages that represent decreasing degrees of partial melting of its mantle source with time. At Jasper, the most voluminous shield building stage was followed by the younger and substantially less voluminous flank series and, finally by the rejuvenated summit alkalic series that are highly enriched in incompatible trace elements (Konter et al., 2009). To a first order, the combined R. Crusoe and A. Selkirk data indicate a history roughly following these stages of Jasper evolution.

The geochemical evolution of R. Crusoe also bears gross similarities with that of Tahaa, the largest of the Society Islands (White and Duncan, 1996). Tahaa has an age range of 2.3 Ma with a volcanic hiatus of 1.2 M.y. between the shield building and post-erosional stages. Although the latter stage in Tahaa has a less-enriched (or relatively depleted) isotopic signature compared to the earlier shield building stage, which is opposite of the shield – rejuvenated (or post-shield) isotopic relationship in Juan Fernandez, the main point is that Society Island lavas were created by two mantle components. As presented earlier, compositional signatures of FOZO and depleted components are recognized in Juan Fernandez lavas (see also, Gerlach et al., 1986; Baker et al., 1987).

Based on the geochemical features of Juan Fernandez lavas and their similarities with other oceanic islands purportedly generated by mantle plumes, together with field observations and petrographic data (Baker et al., 1987; Farley, 1991; Farley et al., 1993; Natland, 2003; Gerlach et al., 1986; Truong, 2015; Reyes et al., 2017), the following model for the geologic evolution of Juan Fernandez volcanic chain is proposed (Fig. 7). The earliest phase is the pre-shield building stage. Magmatism associated with this phase is not well defined, but inferences from other volcanic island chains suggest that this stage most probably erupts a heterogeneous mixture of lavas that precedes the arrival of the main body of an upwelling mantle plume. For example, Devey et al. (2000) reported that magmas from the submarine Friday and Domingo volcanoes are highly alkaline, most probably due to small degrees of partial melting of the plume source. Thus, lavas at this stage have a variable composition because the core component of the plume has not been sampled and/or the main batch of plume melt has not yet impinged the lithosphere. This stage would be represented by the inaccessible, not yet sampled, lowermost structures of both islands and the small, western-most seamounts along the chain.

The next phase is the main shield-building stage and is represented by A. Selkirk Group III basalts. The basalts are produced by a relatively large degree of partial melting of the core of the mantle plume. This is compatible with a previous proposal that the low Ba/Zr ratio A. Selkirk Group III basalts were tapping a source somewhat different from that of R. Crusoe basalts (Farley et al., 1993). At this stage, the mantle plume yields magmas that are mainly tholeiitic to transitional to alkalic basalts with 'relatively depleted' isotopic and incompatible element compositions.

The later phase of the shield-building stage is represented by R. Crusoe Group I basalts. Together with Group III basalts, they comprise the shield unit basalts of Reyes et al. (2017). However, Group I basalts were produced through later, smaller degree of partial melting of the FOZO component of the mantle plume. As smaller degree partial melts, these lavas are relatively enriched in incompatible trace elements than Group III lavas. Finally, the rejuvenated stage is represented by minor intrusives and late volcanics, such as the Group II basanites in R. Crusoe. The latter lavas are the smallest degree partial melts coming from the tail end of the mantle plume, experienced polybaric fractional crystallization (Reyes et al., 2017) and were erupted as parasitic cones and intruded as dikes that cross-cut the underlying shield lavas (Gerlach et al., 1986; Baker et al., 1987; Reyes et al., 2017). Accordingly, they comprise the small volume, more Si-undersaturated and incompatible element-enriched lavas. As Group II lavas intruded pre-existing lava formations, they also exhibit the most alteration or crustal modification features. This is consistent with the slightly higher ^{18}O content of the basanites relative to other Juan Fernandez lavas; a higher than normal ^{18}O content is generally attributed to assimilation of altered lavas from high-levels in the volcanic edifice, assimilation of the oceanic crust underlying the volcano, or incorporation of subducted oceanic crust in mantle sources (Eiler et al., 1997).

5.4. Implications for the variable $^{3}He/^{4}He$ of Juan Fernandez lavas

The ranges of $^{3}He/^{4}He$ in Juan Fernandez lavas are 13.6 to 18.0 R_A

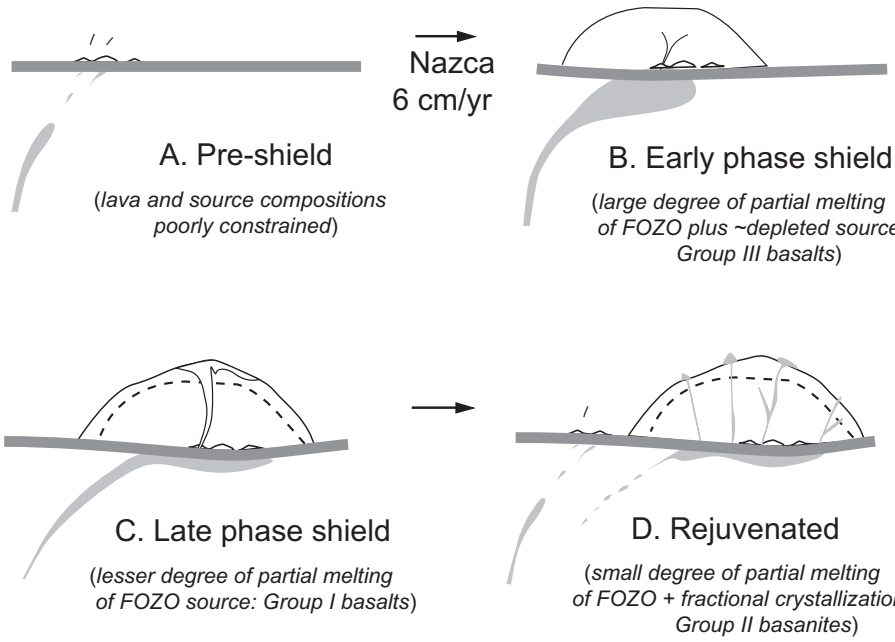

Fig. 7. Proposed stages of the volcanologic evolution of Juan Fernandez Islands. A. Pre-shield, B. Early Phase shield, C. Late Phase shield, D. Rejuvenated (or post-shield). See text for discussion.

in Group I, 11.2–12.5 R_A in Group II and 7.8–9.5 R_A in Group III. To explain the lower $^3He/^4He$ of Group II basanites relative to Group I basalts, Farley et al. (1993) proposed binary mixing between a high-$^3He/^4He$ primitive, undegassed and geochemically enriched Juan Fernandez mantle plume end-member and the geochemically depleted upper mantle, in a fashion like that previously proposed for several Hawaiian volcanoes (Kurz et al., 1983). Notably, however, Farley and co-workers did not propose an asthenospheric origin for the Group III basalts that actually have MORB-like $^3He/^4He$. Moreover, their proposal is clearly at odds with more recent interpretations of available data for the depleted component and variable $^3He/^4He$ nature of the Hawaiian mantle plume. In contrast to the previous idea that the depleted component comes from the asthenosphere (e.g., Kurz et al., 1983; Keller et al., 2000), Regelous et al. (2003; see also Kurz et al., 2004; Frey et al., 2005) proposed that the depleted component is part of the nominally enriched Hawaii mantle plume, similar to proposals for the Galapagos mantle plume (e.g., Hoernle et al., 2000) and Samoan mantle plume (Jackson et al., 2014). The MORB-like (8 ± 1 R_A) $^3He/^4He$ of Hawaiian lavas could therefore be an intrinsic part of the heterogeneous mantle plume (Regelous et al., 2003; Kurz et al., 2004; Frey et al., 2005; see also Hahm et al., 2009). It could also represent a low $^3He/^4He$ residue due to previous degassing (e.g., Hilton et al., 2000; DePaolo et al., 2001) or due to earlier carbonatite melt separation of the high $^3He/^4He$ plume component (Hofmann et al., 2011). Significantly, almost all geochemical tracers indicate a deep mantle plume source for Hawaiian lavas although their $^3He/^4He$ varies from 6 to 34 R_A (e.g., DePaolo et al., 2001; Kurz et al., 2004).

Juan Fernandez exhibits a large range in $^3He/^4He$ similar to Hawaiian lavas despite its limited ranges in $^{87}Sr/^{86}Sr$ and $^{143}Nd/^{144}Nd$ (Fig. 8). Moreover, both their high $^3He/^4He$ lavas are associated with high $^{208}Pb/^{204}Pb$ and low $^{143}Nd/^{144}Nd$ and Zr/Nb relative to other Juan Fernandez (Figs. 2B, 4 and 5) and Mauna Kea lavas (Kurz et al., 2004). Thus, based on major and trace elements, Sr-Nd-Pb isotopes and geologic evolution of the Juan Fernandez linear volcanic chain presented above, as well as on the overall compositional similarity between Juan Fernandez and Hawaiian lavas, we propose that the low (or MORB-like) $^3He/^4He$ is also an intrinsic part of the Juan Fernandez mantle plume. In other words, the low $^3He/^4He$ of Juan Fernandez lavas does not come from the geochemically depleted upper mantle (cf. Farley et al., 1993).

An asthenospheric mantle source for the lower $^3He/^4He$ of Group II basalts is also highly inconsistent with their extreme enrichment in incompatible trace elements and the similarity of their OIB-like Sr-Nd-Pb isotopic signatures with both Groups I and II lavas (Figs. 2 to 5, 8). As discussed in the previous section, rejuvenated Group II basanites were most probably derived later from the same mantle plume source as Group I basalts. Such a source may have upwelled from below and underplated the lithosphere during the transition from shield to rejuvenated stage of the volcanic evolution of Juan Fernandez lavas (Fig. 7). This argument is clearly supported by field observations showing that the Group II basanites, consisting mainly of parasitic cones and dikes intruding basaltic flows, are smaller in volume and ca. 1 M.y. younger than Group I basalts (Baker et al., 1987; see also, Gerlach et al., 1986; Reyes et al., 2017). Being smaller degree partial melts and having suffered polybaric crystal fractionation or olivine accumulation (Fig. 6), Group II basanites contain higher incompatible trace element such as Th and U than Group I basalts. Consequently, high U and Th could have lowered the $^3He/^4He$ ratio in Group II basanites while maintaining a nearly constant Sr-Nd-Pb isotopic composition during the roughly 1 M.y. transition or hiatus from shield to rejuvenated stages. The key issue is whether 1 M.y. is sufficient time to grow-in the requisite ^4He to lower $^3He/^4He$ values. Model calculations (Table 2) using the following equation from Graham et al. (1987):

$$^4He^* = 2.80 \times 10^{-8}\{[U](4.35 + Th/U)\}T(cm^3\ STP\ g^{-1})$$

show that the $^3He/^4He$ (11.2–12.5 R_A) range of Group II basanites can indeed be attained within 1 M.y. from Group I basalt PIN-8 (with an original $^3He/^4He$ of 17.2 R_A) by simply trapping < 3% of $^4He^*$ produced by the high U and Th contents of the Group II basanites. More importantly, degassing of Juan Fernandez volcanoes most probably helped lower the concentration of the original He and, thus, decreased the time required to lower $^3He/^4He$ (e.g., Hilton et al., 2000). In short, the above analyses suggest that it is plausible to produce the lower $^3He/^4He$ values of Group II by radiogenic in-growth ± degassing. If correct, then there is no requirement for the involvement of

Table 2
Per cent ^4He from Group I basalt needed to produce Group II $^3He/^4He$ after 1 M.y. hiatus.

$^3He_{PIN-8}$	$[He]_{PIN-8}$	[He*]	$^3He/^4He$	% He*
cc/g	cc/g	(cc/g)	(R/R_A)	Needed
5.65E − 13	2.69E − 08	3.75E − 07	12.5	1.5
5.65E − 13	2.69E − 08	3.75E − 07	11.2	2.5

Notes: PIN-8 has the highest $^3He/^4He$ (17.2 R/R_A) among Group I samples. He* is the amount of ^4He produced after 1 M.y. using the average U + Th of Group II basanites.

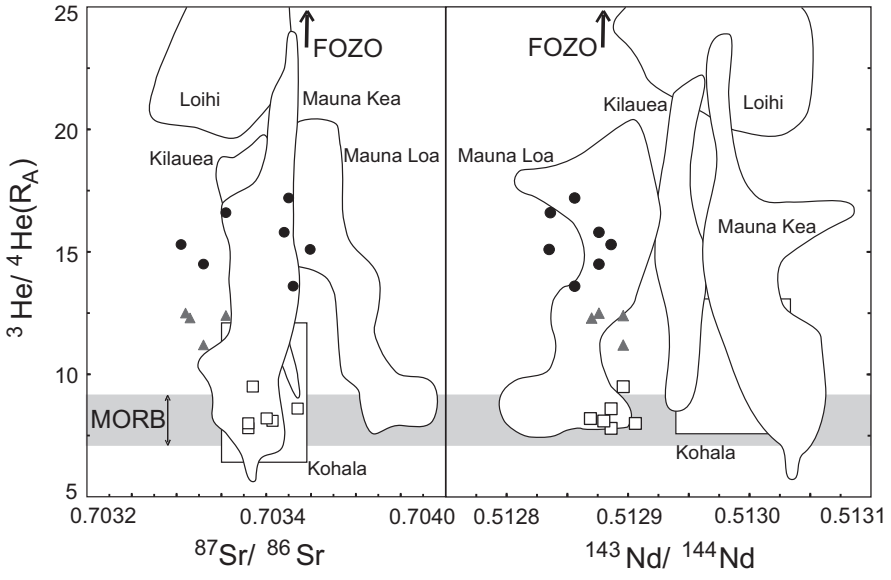

Fig. 8. $^3He/^4He$ (R_A) versus $^{87}Sr/^{86}Sr$ and $^{143}Nd/^{144}Nd$ diagrams for Juan Fernandez lavas. Fields for volcanoes in the island of Hawaii only (after Kurz et al., 2004) are shown for reference. Symbols as in Fig. 4. Note that like Juan Fernandez, individual Hawaiian sample suites have a large range of $^3He/^4He$ (R_A), but limited ranges of $^{87}Sr/^{86}Sr$ and $^{143}Nd/^{144}Nd$. Group II basanites are a subset of Group I that experienced *in situ* production of $^4He^*$ from its U and Th contents. See text for additional discussion.

asthenospheric material in generating the Group II basanites (cf., Farley et al., 1993).

As in the previous Sr-Nd-Pb isotopic argument, the parental magmas for Groups I and II high $^3He/^4He$ lavas originate at or near FOZO as it is the common source of high $^3He/^4He$ (> 9 R_A) OIB (e.g., Hanan and Graham, 1996; Hilton et al., 1999; Castillo, 2015, 2016). Although Group III parental magmas also originate from the same source, the latter has MORB-like $^3He/^4He$ as the Juan Fernandez mantle plume is compositionally heterogeneous and most likely contains a less-enriched or depleted component with lower $^3He/^4He$ (< 9 R_A), similar to, e.g., Mauna Kea. Major and trace element data show that the Juan Fernandez parental magmas were derived though sequential and variable degrees of partial melting of such a common mantle plume source. Initial, relatively large degree of partial melting sampled FOZO plus the depleted component with a MORB-like $^3He/^4He$ of 8 ± 1 R_A, producing Group III basalts whereas later, smaller degree of partial melting sampled mainly the FOZO source with high $^3He/^4He$ > 9 R_A, producing Group I basalts and Group II basanites. In sum, none of the two source components of the Juan Fernandez mantle plume require extreme end-components and instead fall within or close to FOZO.

The above proposal is consistent with the geochemistry of several critical samples. The PV-2 basanitoid is a mixture of basalt and basanite magmas produced during the transition from the climax of the shield-building stage to the rejuvenated stage and, thus, is chemically and isotopically transitional between Groups I and II. Unsurprisingly, PV-2 also has $^3He/^4He$ (13.6 R_A) transitional between Groups I and II (Fig. 2). On the other hand, sample MF-C2, the only Group III sample from A. Selkirk analyzed here that has $^3He/^4He$ higher than the MORB range, at 9.5 R_A, was collected from the island's summit (Farley, 1991; Farley et al., 1993). Hence, it is a young, if not the youngest, eruptive at A. Selkirk and represents the transition from the main shield-building A. Selkirk (or Group III) to late shield-building R. Crusoe (or Group II) stage, whence the more depleted component was generally expended and/or overwhelmed by the influx of higher $^3He/^4He$ FOZO plume component.

Finally, the similarity of the $^{143}Nd/^{144}Nd$ ratios of three out of the five olivines and host rocks (Table 1) suggests that the $^{143}Nd/^{144}Nd$ values preserved by the olivines are in isotopic equilibrium with those in their respective host magmas. That is, the olivine phenocrysts may have equilibrated with the last drop of melts in Juan Fernandez, despite their complex crystallization histories as clearly evidenced in the petrography and chemistry of these olivines (Natland, 2003). Neodymium, similar to He, occurs in trace amounts in olivine as its distribution coefficient in olivine is very low (K_d = 0.006; Rollinson, 1993). The fact that we could measure $^{143}Nd/^{144}Nd$ from the olivine separates indicates that Nd is also trapped like He in crystallizing olivine phenocrysts, as Nd is present in tiny melt inclusions and silicate or spinel crystals trapped inside cavities, bubbles and thermal stress fractures in the olivine (cf., Natland, 2003). On the other hand, the slightly lower $^{143}Nd/^{144}Nd$ ratios (which generally trend toward higher $^3He/^4He$ – Fig. 8; see also, Farley et al., 1993) of two out of the five olivines relative to host rocks may also indicate that the initial primary magma has higher $^3He/^4He$ than the residual differentiated and, most likely, more degassed (e.g., Hilton et al., 2000; DePaolo et al., 2001) melt that crystallized to form the bulk of the rock. Either way, these preliminary results suggest that olivine reflects the inherent heterogeneities of both $^3He/^4He$ and $^{143}Nd/^{144}Nd$ in the source of Juan Fernandez lavas. Thus, the petrographic characteristics of He-bearing olivines generally do not support the idea that the He content (and, hence, e.g. high $^3He/^4He$) of olivines comes from implicitly separate, late-arriving mantle volatiles that permeated into shallow magma reservoirs where magmatic differentiation were fairly extensive (cf., Natland, 2003). Instead, the $^3He/^4He$ and bulk composition of Juan Fernandez lavas reflect those of their source and the differentiation processes experienced by the primary melts derived from this source.

6. Conclusions

This study presents new trace element and Sr, Nd and Pb isotopic analyses of Juan Fernandez lavas to further constrain their petrogenesis and mantle source composition. Variations in major and trace element composition in the lavas are mainly controlled by differences in degrees of partial melting of a common, slightly compositionally heterogeneous mantle source. Overall, major and trace element data and modeling suggest that A. Selkirk Group III basalts were produced by the largest degree of partial melting at moderately low pressure, followed by R. Crusoe Group I basalts. R. Crusoe Group II basanites were produced by the smallest degree of partial melting. Fractional crystallization accounts for some of the compositional variations of the rock groups, particularly those in the R. Crusoe Group II basanites.

The new data confirm the limited range of Sr, Nd and Pb isotopic ratios of Juan Fernandez lavas despite their relatively large range of $^3He/^4He$ values. As with major and trace element analyses, the limited isotopic range of radiogenic isotopes indicates that the parental magmas for Juan Fernandez lavas are derived from a common, though slightly heterogeneous mantle plume source. This source resides at or near the FOZO region inside Sr-Nd-Pb isotopic space. A small but distinct compositional variability exists within this source. A FOZO mantle source, with a young HIMU Pb isotopic composition, is preferentially sampled by R. Crusoe melts whereas A. Selkirk melts sample FOZO with an additional geochemically depleted flavor. Significantly, the observed geochemical variance of Juan Fernandez lavas is consistent with the temporal evolution of Juan Fernandez volcanoes as they progress through shield-building and rejuvenated stages.

Results of the combined major-trace element and Sr-Nd-Pb investigation do not indicate substantial contributions from asthenospheric mantle, and there is little evidence of crustal contamination. Instead, the combined results show that the early phase of shield building stage (Group III lavas) sampled both FOZO and a relatively depleted component with $^3He/^4He$ = 8 ± 1 R_A whereas the later phase sampled (Group I lavas) FOZO component with $^3He/^4He$ > 9 R_A. Group II basanites are late stage Group I lavas that suffered ingrowth of ^4He and, thus, have $^3He/^4He$ lower than Group I, but still higher than Group III. Juan Fernandez is unlike other high $^3He/^4He$ OIB linear volcanic chains because of the dominance of the FOZO mantle plume component in its mantle plume source.

Acknowledgments

We thank J. Konter and an anonymous reviewer for their helpful reviews and comments and C. MacIsaac and L. Finnin for their assistance in the laboratory.

Appendix A. Supplementary data

Supplementary data to this article can be found online at https://doi.org/10.1016/j.chemgeo.2017.11.024.

References

Allègre, C.J., Minster, J.F., 1978. Quantitative models of trace element behavior in magmatic processes. Earth Planet. Sci. Lett. 38, 1–25. http://dx.doi.org/10.1016/0012-821X(78)90123-1.

Baker, P.E., Gledhill, A., Harvey, P.K., Hawkesworth, C.J., 1987. Geochemical evolution of the Juan Fernandez Islands, SE Pacific. J. Geol. Soc. Lond. 144, 933–944. http://dx.doi.org/10.1144/gsjgs.144.6.0933.

Booker, J., Bullard, E.C., Grasty, R.L., 1967. Palaeomagnetism and age of rocks from Easter Island and Juan Fernandez. Geophys. J. Roy. Astr. Soc. 12, 469–471. http://dx.doi.org/10.1111/j.1365-246X.1967.tb03127.x.

Castillo, P.R., 2015. The recycling of marine carbonates and sources of HIMU and FOZO ocean island basalts. Lithos 216, 254–263. http://dx.doi.org/10.1016/j.lithos.2014.12.005.

Castillo, P.R., 2016. A proposed new approach and unified solution to old Pb paradoxes. Lithos 252, 32–40. http://dx.doi.org/10.1016/j.lithos.2016.02.015.

Castillo, P.R., 2017. An alternative explanation for the Hf-Nd mantle array. Sci. Bull. 62,

974–975.
Castillo, P.R., Scarsi, P., Craig, H., 2007. He, Sr, Nd, and Pb isotopic constraints on the origin of the Marquesas and other linear volcanic chains. Chem. Geol. 240 (3), 205–221. http://dx.doi.org/10.1016/j.chemgeo.2007.02.012.
Corvalan, J., 1981. Plate Tectonic Map of the Circum-Pacific Region, Southeast Quadrant.
Craig, H., Lupton, J.E., 1976. Primordial neon, helium, and hydrogen in oceanic basalts. Earth Planet. Sci. Lett. 31, 369–385.
Craig, H., Lupton, J.E., 1981. Helium-3 and mantle volatiles in the ocean and the oceanic crust. In: Emiliani, C. (Ed.), The Sea. 7. Wiley, New York, pp. 391–428.
Day, J.M.D., Pearson, D.G., Macpherson, C.G., Lowry, D., Carracedo, J.C., 2010. Evidence for distinct proportions of subducted oceanic crust and lithosphere in HIMU-type mantle beneath El Hierro and La Palma, Canary Islands. Geochim. Cosmochim. Acta 74, 6565–6589.
DePaolo, D.J., Bryce, J.G., Dodson, A., Schuster, D.L., Kennedy, B.M., 2001. Isotopic evolution of Mauna Loa and the chemical structure of the Hawaiian plume. Geochem. Geophys. Geosyst. 2 (2000GC000139).
Devey, C.W., Hémond, C., Stoffers, P., 2000. Metasomatic reactions between carbonated plume melts and mantle harzburgite: the evidence from Friday and Domingo Seamounts (Juan Fernandez chain, SE Pacific). Contrib. Mineral. Petrol. 139, 68–84. http://dx.doi.org/10.1007/s004100050574.
Eiler, J.M., Farley, K.A., Valley, J.W., Hauri, E., Craig, H., Hart, S.R., Stolper, E.M., 1997. Oxygen isotope variations in ocean island basalt phenocrysts. Geochim. Cosmochim. Acta 61, 2281–2293. http://dx.doi.org/10.1016/S0016-7037(97)00075-6.
Farley, K.A., 1991. Rare Gases and Radiogenic Isotopes in South Pacific Ocean Island Basalts (Ph.D. Thesis). University of California.
Farley, K.A., Natland, J.H., Craig, H., 1992. Binary mixing of enriched and undegassed (primitive?) mantle components (He, Sr, Nd, Pb) in Samoan lavas. Earth Planet. Sci. Lett. 111, 183–199. http://dx.doi.org/10.1016/0012-821X(92)90178-X.
Farley, K.A., Basu, A.R., Craig, H., 1993. He, Sr and Nd isotopic variations in lavas from the Juan-Fernandez Archipelago, SE Pacific. Contrib. Mineral. Petrol. 115, 75–87. http://dx.doi.org/10.1007/BF00712980.
Feigenson, M.D., Hofmann, A.W., Spera, F.J., 1983. Case studies on the origin of basalt. Contrib. Mineral. Petrol. 84 (4), 390–405. http://dx.doi.org/10.1007/BF01160290.
Foulger, G.R., 2011. Plates vs. Plumes: A Geological Controversy. John Wiley & Sons, Chichester.
Frey, F.A., Huang, S., Blichert-Toft, J., Regelous, M., Boyet, M., 2005. Origin of depleted components in basalt related to the Hawaiian hot spot: evidence from isotopic and incompatible element ratios. Geochem. Geophys. Geosyst. 6, Q02L07. http://dx.doi.org/10.1029/2004GC000757.
Gast, P.W., Tilton, G.R., Hedge, C., 1964. Isotopic composition of lead and strontium from Ascension and Gough Islands. Science 145 (3637), 1181–1185. http://dx.doi.org/10.1126/science.145.3637.1181.
Gerlach, D.C., Hart, S.R., Morales, V.W.J., Palacios, C., 1986. Mantle heterogeneity beneath the Nazca plate: San Felix and Juan Fernandez islands. Nature 322, 165–169. http://dx.doi.org/10.1038/322165a0.
Graham, D.W., 2002. Noble gas isotope geochemistry of mid-ocean ridge and ocean island basalts: characterization of mantle source reservoirs. Rev. Mineral. Geochem. 47, 247–317. http://dx.doi.org/10.2138/rmg.2002.47.8.
Graham, D.W., Jenkins, W.J., Kurz, M.D., Batiza, R., 1987. Helium isotope disequilibrium and geochronology of glassy submarine basalts. Nature 326, 384–386.
Gripp, A.E., Gordon, R.G., 2002. Young tracks of hotspots and current plate velocities. Geophys. J. Int. 150 (2), 321–361. http://dx.doi.org/10.1046/j.1365-246X.2002.01627.x.
Hahm, D., Castillo, P.R., Hilton, D.R., 2009. A deep mantle source for high $^{3}He/^{4}He$ ocean island basalts (OIB) inferred from Pacific near-ridge seamount lavas. Geophys. Res. Lett. 36 (2), L20316. http://dx.doi.org/10.1029/2009GL040560.
Hanan, B.B., Graham, D.W., 1996. Lead and helium isotope evidence from oceanic basalts for a common deep source of mantle plumes. Science 272 (5264), 991–995. http://dx.doi.org/10.1126/science.272.5264.991.
Hart, S.R., 1984. A large-scale isotope anomaly in the Southern Hemisphere mantle. Nature 309, 753–757. http://dx.doi.org/10.1038/309753a0.
Hart, S.R., Hauri, E.H., Oschmann, L.A., Whitehead, J.A., 1992. Mantle plumes and entrainment: isotopic evidence. Science 256 (5056), 517–520. http://dx.doi.org/10.1126/science.256.5056.517.
Hauri, E.H., Whitehead, J.A., Hart, S.R., 1994. Fluid dynamic and geochemical aspects of entrainment in mantle plumes. J. Geophys. Res. 99, 24,275–24,300.
Hilton, D.R., Porcelli, D., 2014. Noble gases as tracers of mantle processes. In: Carlson, R.L. (Ed.), The Mantle and Core Vol. 3, Treatise on Geochemistry, 2nd edition (Eds. Turekian, K.K., Holland, H.D.). Elsevier-Pergamon, Oxford, UK, pp. 327–353.
Hilton, D.R., Gronvold, K., Macpherson, C.G., Castillo, P.R., 1999. Extreme $^{3}He/^{4}He$ ratios in northwest Iceland: constraining the common component in mantle plumes. Earth Planet. Sci. Lett. 173, 53–60.
Hilton, D.R., Macpherson, C.G., Elliott, T.R., 2000. Helium isotope ratios in mafic phenocrysts and geothermal fluids from La Palma, the Canary Islands (Spain): implications for HIMU mantle sources. Geochim. Cosmochim. Acta 64, 2119–2132.
Hoernle, K., Reinhard, W., Morgan, J.P., Garbe-Schönberg, D., Bryce, J., Mrazek, J., 2000. Existence of complex spatial zonation in the Galápagos plume. Geology 28 (5), 435–438. http://dx.doi.org/10.1130/0091-7613(2000)28<435:EOCSZI>2.0.CO;2.
Hofmann, A.W., 1997. Mantle geochemistry: the message from oceanic volcanism. Nature 385 (6613), 219–229. http://dx.doi.org/10.1038/385219a0.
Hofmann, A.W., 2014. Sampling Mantle Heterogeneity through Oceanic Basalts: Isotopes and Trace Elements, 2nd ed. Treatise Geochem 3. pp. 67–101.
Hofmann, A.W., Farnetani, C.G., Spiegelman, M., Class, C., 2011. Displaced helium and carbon in the Hawaiian plume. Earth Planet. Sci. Lett. 312, 226–236. http://dx.doi.org/10.1016/j.epsl.2011.09.041.
Jackson, M.G., Hart, S.R., Saal, A.E., Shimizu, N., Kurz, M.D., Blusztajn, J.S., Skovgaard, A.C., 2008. Globally elevated titanium, tantalum, and niobium (TITAN) in ocean island basalts with high $^{3}He/^{4}He$. Geochem. Geophys. Geosyst. 9, Q04027. http://dx.doi.org/10.1029/2007GC001876.
Jackson, M.G., Hart, S.R., Konter, J.G., Kurz, M.D., Blusztajn, J., Farley, K., 2014. Helium and lead isotopes reveal the geochemical geometry of the Samoan plume. Nature 514, 355–358.
Janney, P.E., Castillo, P.R., 1996. Basalts from the Central Pacific Basin: evidence for the origin of Cretaceous igneous complexes in the Jurassic western Pacific. J. Geophys. Res. 101 (B2), 2875–2893. http://dx.doi.org/10.1029/95JB03119.
Kay, R., Hubbard, N.J., Gast, P.W., 1970. Chemical characteristics and origin of oceanic ridge volcanic rocks. J. Geophys. Res. 75 (8), 1585–1613. http://dx.doi.org/10.1029/JB075i008p01585.
Keller, R.A., Fisk, M.R., White, W.M., 2000. Isotopic evidence for Late Cretaceous plume–ridge interaction at the Hawaiian hotspot. Nature 405 (6787), 673–676. http://dx.doi.org/10.1038/35015057.
Klein, E.M., Langmuir, C.H., 1987. Global correlations of ocean ridge basalt chemistry with axial depth and crustal thickness. J. Geophys. Res. 92 (B8), 8089–8115. http://dx.doi.org/10.1029/JB092iB08p08089.
Konter, J.G., Staudigel, H., Blichert-Toft, J., Hanan, B.B., Polvé, M., Davies, G., Shimizu, N., Schiffman, P., 2009. Geochemical stages at Jasper Seamount and the origin of intraplate volcanoes. Geochem. Geophys. Geosyst. 10 (2), Q02001. http://dx.doi.org/10.1029/2008GC002236.
Kurz, M.D., Jenkins, W.J., Hart, S.R., Clague, D., 1983. Helium isotopic variations in volcanic rocks from Loihi Seamount and the Island of Hawaii. Earth Planet. Sci. Lett. 66, 388–406. http://dx.doi.org/10.1016/0012-821X(83)90154-1.
Kurz, M.D., Curtice, J., Lott, D.E., Solow, A., 2004. Rapid helium isotopic variability in Mauna Kea shield lavas from the Hawaiian Scientific Drilling Project. Geochem. Geophys. Geosyst. 5 (4), Q04G14. http://dx.doi.org/10.1029/2002GC000439.
Morgan, W.J., 1972. Deep mantle convection plumes and plate motions. AAPG Bull. 56 (2), 203–213.
Natland, J.H., 2003. Capture of helium and other volatiles during the growth of olivine phenocrysts in picritic basalts from the Juan Fernandez Islands. J. Petrol. 44 (3), 421–456. http://dx.doi.org/10.1093/petrology/44.3.421.
Niu, Y., O'Hara, M.J., 2008. Global correlations of ocean ridge basalt chemistry with axial depth: a new perspective. J. Petrol. 49 (4), 633–664. http://dx.doi.org/10.1093/petrology/egm051.
Peters, B.J., Day, J.M.D., 2014. Assessment of relative Ti, Ta, and Nb (TITAN) enrichments in ocean island basalts. Geochem. Geophys. Geosyst. 15 (11), 4424–4444. http://dx.doi.org/10.1002/2014GC005506.
Regelous, M., Hofmann, A.W., Abouchamis, W., Galer, J.G., 2003. Geochemistry of lavas from the Emperor Seamounts, and the geochemical evolution of Hawaiian magmatism from 85 to 42 Ma. J. Petrol. 44 (1), 113–140. http://dx.doi.org/10.1093/petrology/44.1.113.
Reyes, J., Lara, L.E., Morata, D., 2017. Contrasting P-T paths of shield and rejuvenated volcanism at Robinson Crusoe Island, Juan Fernández Ridge, SE Pacific. J. Volc. Geotherm. Res. 341, 242–254.
Rodrigo, C., Lara, L.E., 2014. Plate tectonics and the origin of the Juan Fernández Ridge: analysis of bathymetry and magnetic patterns. Lat. Am. J. Aquat. Res. 42 (4), 907–917. http://dx.doi.org/10.3856/vol42-issue4-fulltext-15.
Rollinson, H.R., 1993. Using Geochemical Data: Evaluation, Presentation, Interpretation. Longman Group UK Ltd., London.
Stracke, A., 2012. Earth's heterogeneous mantle: a product of convection-driven interaction between crust and mantle. Chem. Geol. 330, 274–299. http://dx.doi.org/10.1016/j.chemgeo.2012.08.007.
Stracke, A., Hofmann, A.W., Hart, S.R., 2005. FOZO, HIMU, and the rest of the mantle zoo. Geochem. Geophys. Geosyst. 6, Q05007. http://dx.doi.org/10.1029/2004GC000824.
Stuart, F.M., Lass-Evans, S., Fitton, J.G., Ellam, R.M., 2003. High $^{3}He/^{4}He$ ratios in picritic basalts from Baffin Island and the role of a mixed reservoir in mantle plumes. Nature 424, 57–59. http://dx.doi.org/10.1038/nature01711.
Stuessy, T.F., Foland, K.A., Sutter, J.F., Sanders, R.W., Silva, M., 1984. Botanical and geological significance of potassium-argon dates from the Juan Fernandez Islands. Science 225 (80), 49–51. http://dx.doi.org/10.1126/science.225.4657.49.
Sun, S.-S., McDonough, W.F., 1989. Chemical and isotopic systematics of oceanic basalts: implications for mantle composition and processes. In: Saunders, A.D., Norry, M.J. (Eds.), Magmatism in the Ocean Basins. Geological Society Special Publication, London, vol. 42. pp. 313–345. http://dx.doi.org/10.1144/GSL.SP.1989.042.01.19.
Thirlwall, M.F., 1997. Pb isotopic and elemental evidence for OIB derivation from young HIMU mantle. Chem. Geol. 139 (1), 51–74. http://dx.doi.org/10.1016/S0009-2541(97)00033-8.
Truong, T.B., 2015. Trace Element Abundances and Sr-Nd-Pb Isotopic Constraints on the Petrogenesis of Juan Fernandez Lavas (MS Thesis). University of California, San Diego (59 pp.).
Vidal, P., 1992. Mantle: more HIMU in the future? Geochim. Cosmochim. Acta 56, 4295–4299.
White, W.M., 2015. Isotope Geochemistry. John Wiley & Sons, Chichester.
White, W.M., Duncan, R.A., 1996. Geochemistry and geochronology of the Society Islands: new evidence for deep mantle recycling. Geophys. Monogr. Ser. 95, 183–206.
Wilson, J.T., 1963. A possible origin of the Hawaiian islands. Can. J. Phys. 41, 863–870. http://dx.doi.org/10.1139/p63-094.
Zindler, A., Hart, S., 1986. Chemical geodynamics. Annu. Rev. Earth Planet. Sci. 14, 493–571.